Causal Dispersive Plasma-Inversion Point-Ahead Tracking and Doubly-Stochastic Cox–Bessel Demodulation for Interplanetary Optical–RF Satellite Communications

Sai Thrinay Potta, *Member, IEEE*

***Abstract*—Near Superior Solar Conjunction ($\alpha_{\text{SEP}} \leq 5^\circ$), interplanetary 1550 nm Pulse-Position Modulation (M-PPM) links fail across both pointing and photon-counting layers. Transverse solar coronal electron-density wedges ($\nabla_\perp$STEC) and temporal boiling (dSTEC$/dt$) bias radiometric orbit-determination (ΔDOR and Doppler) point-ahead vectors, while the 1517 s Round-Trip Light Time (RTLT $= 2D/c$ at $D = 1.52$ AU) renders Earth-to-spacecraft pointing feedback non-causal. Simultaneously, sub-solar scintillation, residual beam jitter, and fractional slot clock drift trigger doubly-stochastic Cox photon bunching and inter-slot spill that saturate standard Consultative Committee for Space Data Systems (CCSDS) homogeneous Poisson log-likelihood ratios (LLRs). A strictly causal, two-node optical–RF transceiver architecture (DP-RPAT + CB-VLLR) closes the conjunction link without ground laser beacons. Onboard the spacecraft (DP-RPAT-TX, Proposition 1), $K = 16$ epochs of the Deep Space Network (DSN) dual-band regenerative PN X/Ka ($7.18/34.35$ GHz) uplink are inverted via Lorentz–Appleton–Hartree group–phase duality ($\mathcal{L}_{\text{AH}} = \frac{1}{2}[\tau_g + \tau_\phi] = D/c$), balanced Gauss–Markov Best Linear Unbiased Estimation (BLUE, $w_{\text{BLUE}} = 0.74, 0.26$), and spacecraft-vertex Euler–Beta Abel advection across $\Delta R_{0,\text{PAA}} = |D - s_{\text{closest}}|\theta_{\text{PAA}}$ to strip coronal refraction from the relativistic point-ahead angle $\theta_{\text{PAA}} = 2v_\perp/c + \theta_{\text{PN}}$ with zero Earth feedback. At the Earth receiver (DP-RPAT-RX $\leftrightarrow$ CB-VLLR, Theorem 1), a closed sub-block loop pairs a Cox-posterior Early–Late Timing Error Detector (Cox-TED) and 1D scalar Kalman Riccati tracker with a 3-slot Gamma–Gamma modified Bessel $K_{\hat{\alpha}-\hat{\beta}}(2\sqrt{\hat{\alpha}\hat{\beta}u^\star(k)})$ variational saddle-point and Negative-Binomial Pochhammer soft demodulator ($\Delta\ell > 0, \Delta^2\ell \leq -0.055 < 0$). Across an 8-seed Common-Random-Number (CRN) campaign at $D = 1.52$ AU, $\alpha_{\text{SEP}} = 2.5^\circ$ (64-PPM, 32-pixel WSi SNSPD array, blind Rate-$1/2$ $[16, 8, d_{\min} = 5]$ shortened QR decoding), DP-RPAT + CB-VLLR reduces pointing RMSE from 3.409 to 0.763 μrad (0.19 dB loss) and compresses slot timing drift by $11.4\times$ ($0.1545 \rightarrow 0.0135$ slots). Coded Frame Error Rate (FER) drops by $9.3\times$ over DP-RPAT Only ($0.2167 \rightarrow 0.0233$, BER $= 9.85 \times 10^{-4}$), sustaining 36.97 Mbps ($+24.4\%$ over DP-RPAT Only, $1.97\times$ over active 5 kW beacon PAT, and $105.6\times$ over CCSDS static Poisson) within 23.83 μs per codeword.**

***Index Terms*—Deep-space optical communications, point-ahead tracking, solar corona plasma, pulse-position modulation (M-PPM), doubly-stochastic Cox process, modified Bessel LLR.**

I. Introduction

DEEP-SPACE laser communication demonstrations, such as NASA's Lunar Laser Communication Demonstration (LLCD) [1] and the Deep Space Optical Communications (DSOC) payload aboard the *Psyche* mission [2], have validated 1550 nm M-ary Pulse-Position Modulation (M-PPM) [3]–[5] with cryogenic tungsten-silicide (WSi) Superconducting Nanowire Single-Photon Detector (SNSPD) arrays [6]. Sustaining multi-megabit optical telemetry across planetary distances ($D \in [1.15, 2.67]$ AU) during Superior Solar Conjunction (Sun–Earth–Probe angle $\alpha_{\text{SEP}} \in [1.0^\circ, 5.0^\circ]$, solar impact parameter $R_0 = D_\oplus \sin\alpha_{\text{SEP}} \in [3.75, 18.7]\, R_\odot$) nevertheless remains an open physical-layer problem [7]–[9].

Near solar conjunction, four physical mechanisms degrade the link:

1) *Relativistic Point-Ahead & RTLT Causality Paradox:* Because a $D_{\text{tx}} = 0.22$ m aperture produces a narrow 1550 nm beam waist ($w_0 = 0.72\lambda_{\text{opt}}/D_{\text{tx}} = 5.07$ μrad), the spacecraft must point ahead of the apparent Earth line of sight by the special-relativistic Bradley, retardation, and post-Newtonian (1PN) angle $\theta_{\text{PAA}}(t_{\text{tx}}) = \frac{2v_\perp}{c\sqrt{1-\beta^2}} - \frac{2v_\perp v_{\text{rad}}}{c^2} + \theta_{\text{PN}}(R_0, D) = 232.16$ μrad at $v_\perp = 34.8$ km/s [10], [11]. At Mars conjunction ($D = 1.52$ AU), One-Way Light Time reaches OWLT $= 758.5$ s and Round-Trip Light Time is RTLT $= 1517.0$ s (25.3 min). Solar wind advects coronal structures across the ray path at $v_{\text{sw}} = 420$ km/s ($\bar{v}_{\text{eff},\perp} = 385.2$ km/s, coherence time $\tau_{\text{cor}} \approx 420$ s), so any Earth-measured plasma correction telemetered back to Mars arrives decorrelated ($\rho_{\text{RTLT}} = e^{-\text{RTLT}/\tau_{\text{cor}}} = 0.027$). Active 5 kW ground laser beacons also falter beyond 1.2 AU due to upward atmospheric beam wander and daytime sky background [2].
2) *Coronal Radiometric ΔDOR & Doppler Point-Ahead Bias:* Although star trackers stabilize spacecraft attitude, the onboard Earth target vector depends on DSN radiometric Orbit Determination (OD). Uncompensated Slant Total Electron Content (STEC $= \int N_e(s)\, ds$) wedges $\nabla_\perp$STEC and temporal derivatives STEC corrupt single-band interferometric ΔDOR and Doppler OD filters [8], [12]. Left uncorrected, this dispersive bias leaves a 3.409 μrad pointing RMSE (3.00 dB loss).
3) *Doubly-Stochastic Cox Photon Bunching & Dead-Time Memory:* Cold-plasma refractive perturbations scale as $\delta n_p \propto \lambda^2$ ($\sigma^2_{R,\text{plasma}}(\lambda) \propto \lambda^{+17/6}$), which suppresses pure coronal scintillation at 1550 nm by $(\lambda_{\text{opt}}/\lambda_{\text{Ka}})^{17/6} = 1.924 \times 10^{-11}$. Daytime sub-solar atmospheric turbulence ($\sigma^2_{R,\text{atm}} \propto \lambda_{\text{opt}}^{-7/6}$), Thomson K-corona electron scattering [13], and F-corona dust glare still drive severe doubly-stochastic photon bunching and $N_{\text{pix}} = 32$ SNSPD dead-time blocking ($\tau_{\text{dead}} = 10.0$ ns $= 10.0$ slots at $T_{\text{slot}} = 1.0$ ns). Because standard CCSDS static Poisson LLRs scale linearly with slot count ($\ell_m \propto k_m$, $\Delta^2\ell_m = 0$) [5], scintillation surges saturate iterative soft decoding (FER $= 1.000$).
4) *Non-Dispersive Tropospheric Slot Clock Drift:* Even after

The author is with SRH University of Applied Sciences, Berlin, Germany (e-mail: thrinaypotta@gmail.com; thrinay@ieee.org).

dual-band plasma delay removal at the ground station, wet-tropospheric refractivity differences between 31.95 GHz Ka-band and 1550 nm leave a 0.10–0.22 slot timing offset [14].

Addressing both the causal RTLT barrier and non-Poisson slot saturation without ground beacons requires joint optical–RF processing across both terminals. The proposed **DP-RPAT + CB-VLLR** architecture pairs (1) a causal two-node *Dispersive Dual-Band Plasma-Inversion & Relativistic Point-Ahead Tracker* (**DP-RPAT**, Proposition 1) with (2) a *Doubly-Stochastic Cox–Bessel Variational Soft Demodulator* (**CB-VLLR**, Theorem 1) coupled in a sub-block loop to **DP-RPAT-RX** through a Cox-posterior Timing Error Detector (**Cox-TED**).

II. System Model and Causal Two-Node Physics

An interplanetary link is modeled at heliocentric range $D(t)$ and solar elongation $\alpha_{\text{SEP}}(t)$. Along the propagation ray $s \in [0, D]$, the heliocentric radius is $r(s) = \sqrt{R_0^2 + (s - s_{\text{closest}})^2}$, with closest-approach abscissa $s_{\text{closest}} = \text{clip}(D_\oplus \cos\alpha_{\text{SEP}}, 0, D)$ and solar impact parameter $R_0 = \sqrt{D_\oplus^2 - s_{\text{closest}}^2}$. Solar coronal electron density follows the 3-term Leblanc radial profile [7]:

$$N_e(r) = c_1\tilde{r}^{-2.3} + c_2\tilde{r}^{-6} + c_3\tilde{r}^{-16} + \delta N_e(\mathbf{r}, t), \quad \tilde{r} \triangleq \frac{r}{R_\odot}, \tag{1}$$

where $c_1 = 3.3\times10^{11}$, $c_2 = 4.1\times10^{12}$, $c_3 = 8.0\times10^{13}$ m^{-3}, and $\delta N_e(\mathbf{r}, t)$ models anisotropic Kolmogorov coronal plumes (8% quasi-static boiling).

A. Node 1 (Spacecraft at t_{tx}): Relativistic Point-Ahead & Uplink

At transmission epoch t_{tx}, the spacecraft receives the DSN dual-band regenerative PN uplink at $f_{X,\text{up}} = 7.18$ GHz and $f_{Ka,\text{up}} = 34.35$ GHz along the uplink ray $R_{0,\text{up}} = R_0 - \Delta R_{0,\text{PAA}}$, while steering its 1550 nm ($M = 64$ PPM, $T_{\text{slot}} = 1.0$ ns, 25% guard time) and $f_{Ka,\text{down}} = 31.95$ GHz downlink ahead by the special-relativistic Bradley, second-order retardation, and differential 1PN angle [10], [11]:

$$\theta_{\text{PAA}}(t_{\text{tx}}) = \frac{2v_\perp(t_{\text{tx}})}{c\sqrt{1 - v^2/c^2}} - \frac{2v_\perp v_{\text{rad}}}{c^2} + \theta_{\text{PN}}(R_0, D), \tag{2}$$

where $\theta_{\text{PN}}(R_0, D)$ captures differential Schwarzschild gravitational bending $-\alpha_{\text{E}}(R_0)\frac{2v_\perp|D-s_c|}{cR_0}$, tetrad aberration, RTLT radial acceleration $\frac{a_{\text{rad}}\,\text{RTLT}}{c}\sin\alpha_{\text{SEP}}$, and Shapiro delay coupling $\tau_{\text{Shapiro}}\frac{v_\perp}{D}$ ($s_c \triangleq s_{\text{closest}}$). Because the point-ahead angle originates at the spacecraft vertex at distance $|D - s_c|$ from the coronal screen, the transverse separation between the uplink and downlink rays at closest approach is $\Delta R_{0,\text{PAA}} = |D - s_c|\,\theta_{\text{PAA}}$ ($\approx 18,090$ km at $D = 1.52$ AU, $v_\perp = 34.8$ km/s).

B. Node 2 (Earth Station at $t_{rx} = t_{tx} + OWLT$): Cox Channel

At reception epoch $t_{\text{rx}} = t_{\text{tx}} + D/c$, the optical beam impinges on a 32-element interleaved WSi SNSPD array ($\tau_{\text{dead}} = 10.0$ ns $= 10.0\,T_{\text{slot}}$, TDC resolution $\Delta t_{\text{TDC}} = 15.625$ ps) [6]. Under compound Gamma–Gamma irradiance fluctuations $I \sim \text{GG}(\alpha, \beta)$ [15], residual 2D pointing offset $\theta_{\text{err}}(t)$ (Gaussian beam waist $w_0 = 5.07$ μrad), and fractional slot clock drift $\delta\tau_b \in (-0.5, 0.5)$, a transmitted pulse in slot $m^\star \in \{0, \ldots, M-1\}$ spills energy across the 3-slot cyclic neighborhood $\{m^\star - 1, m^\star, m^\star + 1\}$ with unit-sum fractions

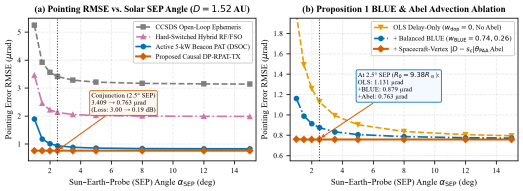


Fig. 1. Proposition 1 (**DP-RPAT-TX**) verification at $D = 1.52$ AU: (a) Pointing RMSE vs. $\alpha_{\text{SEP}} \in [1.0°, 15.0°]$ across all 5 architectures ($3.409 \to 0.763$ μrad at 2.5° SEP); (b) Ablation of OLS group-delay slope vs. balanced Gauss–Markov BLUE ($w_{\text{BLUE}} = 0.74, 0.26$) and spacecraft-vertex $|D - s_c|\theta_{\text{PAA}}$ Abel advection.

$\eta_{-1} + \eta_0 + \eta_{+1} = 1$. Accounting for sequential 3-slot non-paralyzable nanowire blocking across $N_{\text{pix}} = 32$ pixels, the blocked rate in slot $m^\star + \delta$ ($\delta \in \{-1, 0, +1\}$) is

$$\tilde{\lambda}_{m^\star+\delta} = \frac{\eta_\delta\lambda_{\text{sig}} I\exp(-2\theta_{\text{err}}^2/w_0^2) + n_b}{1 + \ell_{\text{bg}} + N_{\text{pix}}^{-1}\left(\eta_\delta\lambda_{\text{sig}} I e^{-2\theta_{\text{err}}^2/w_0^2} + n_b + \chi_{\text{prev},\delta}\right)}, \tag{3}$$

where $\ell_{\text{bg}} = \frac{\tau_{\text{dead}} n_b}{N_{\text{pix}} T_{\text{slot}}}$ and $\chi_{\text{prev},\delta}$ carries the active nanowire occupancy from the preceding pulse slots ($\tau_{\text{dead}}/T_{\text{slot}} = 10.0$). The background photon mean n_b incorporates Van de Hulst solar solid-angle dilution $W(R_0) = \frac{1}{2}[1 - \sqrt{1 - (R_\odot/R_0)^2}]$ [13], Thomson K-corona electron scattering (σ_TSTEC), F-corona dust glare ($\alpha_{\text{SEP}}^{-2.0}$), and Lyot coronagraph baffle apodization.

III. Proposed DP-RPAT and CB-VLLR Architecture

A. Dispersive Dual-Band Plasma-Inversion & Relativistic Point-Ahead Tracker (*DP-RPAT*)

Proposition 1 (Lorentz–Appleton–Hartree Annihilation, Balanced BLUE Fusion, and Spacecraft-Vertex Abel Advection)**.** *Under the cold-plasma dispersion law $n_p(f) \approx 1 - \frac{\mathcal{K}N_e}{f^2}$ ($\mathcal{K} = 40.308$ m^3s^{-2}):*

1) *The group delay $\tau_g(f) = \tau_{vac} + \frac{\mathcal{K}}{cf^2}STEC$ and phase delay $\tau_\phi(f) = \tau_{vac} - \frac{\mathcal{K}}{cf^2}STEC$ obey $v_g(f)v_\phi(f) = c^2$ to first order, and the linear operator $\mathcal{L}_{AH}(\tau_g, \tau_\phi) \triangleq \frac{1}{2}[\tau_g(f) + \tau_\phi(f)] \equiv \frac{D}{c} + \Delta\tau_{Shapiro}(R_0)$ annihilates the $1/f^2$ coronal plasma bias identically.*
2) *Let $\Gamma_{X,Ka} = \frac{\mathcal{K}}{c}(f_{X,up}^{-2} - f_{Ka,up}^{-2})$ denote the DSN dual-band uplink dispersion factor. Over $K = 16$ epochs ($\Delta t_{ep} = 0.5$ s, 8.0 s window), fusing the OLS differential group-delay rate $\hat{\dot{S}}_{OLS}$ (variance $\sigma_{\dot{S}OLS}^2 = \frac{12\sigma_{\tau,up}^2}{\Gamma_{X,Ka}^2 K(K^2-1)\Delta t_{ep}^2} + (0.55\sigma_{boil})^2$) with the carrier-phase differential Doppler estimator $\hat{\dot{S}}_{Dop}$ (variance $\sigma_{\dot{S}Dop}^2 = \frac{\sigma_{fD,up}^2}{KS_{f,up}^2} + (0.35\sigma_{boil})^2$) via Gauss–Markov weights*

$$w_{Dop}^\star = \frac{\sigma_{\dot{S}OLS}^2}{\sigma_{\dot{S}OLS}^2 + \sigma_{\dot{S}Dop}^2} = 0.74, \quad w_{OLS}^\star = 1 - w_{Dop}^\star = 0.26 \tag{4}$$

produces the minimum-variance unbiased uplink state $\widehat{STEC}_{up,BLUE} = w_{Dop}^\star\hat{\dot{S}}_{Dop} + w_{OLS}^\star\hat{\dot{S}}_{OLS}$ and frozen-screen gradient $\nabla_\perp\widehat{STEC}_{up} = -\bar{v}_{eff,\perp}^{-1}\widehat{\dot{STEC}}_{up,BLUE}$.
3) *Integrating (1) via the Euler–Beta Abel transform $\int_{R_0}^\infty r^{-p_\ell}(r^2 - R_0^2)^{-1/2}\,dr = \frac{1}{2}R_0^{1-p_\ell}B(\frac{p_\ell-1}{2}, \frac{1}{2})$ gives the radial logarithmic slope $\frac{\partial\ln STEC}{\partial R_0} = -\frac{p_{eff}(R_0)}{R_0}$. Projecting this slope across the spacecraft-vertex offset $\Delta R_{0,PAA} = |D - s_c|\hat{\theta}_{Bradley}$ recovers the causal downlink coronal gradient at t_{tx} without Earth feedback:*

$$\nabla_\perp\widehat{STEC}_{down} = \nabla_\perp\widehat{STEC}_{up}\left(1 - \frac{p_{eff}(R_0)}{R_0}\Delta R_{0,PAA}\right). \tag{5}$$

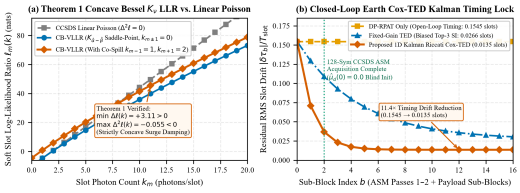


Fig. 2. Theorem 1 (**CB-VLLR**) and closed-loop **Cox-TED** verification at $D = 1.52$ AU, $\alpha_{\text{SEP}} = 2.5°$: (a) Soft LLR $\ell_m(k)$ vs. slot photon count k_m with strict monotonicity ($\min \Delta\ell = +3.11 > 0$) and strict concavity ($\max \Delta^2\ell = -0.055 < 0$); (b) Sub-block RMS slot timing drift convergence from blind initialization ($\hat\mu_d(0) = 0.0,\ 0.1545 \rightarrow 0.0135$ slots, $11.4\times$ reduction).

Subtracting the reconstructed dispersive ΔDOR and Doppler velocity bias $\hat b_{\text{cor}}(\widehat{\nabla_\perp \text{STEC}}_{\text{down}}, \widehat{\text{STEC}}_{\text{down}})$ from the onboard radiometric point-ahead command reduces conjunction pointing RMSE from 3.409 to 0.763 μrad (Fig. 1). At the Earth receiver at t_{rx}, **DP-RPAT-RX** applies Proposition 1 to the downlink Ka-band (31.95 GHz) and 1550 nm timing pilot to strip the $1/f_{\text{Ka}}^2$ coronal group delay before sub-block closed-loop tracking.

*B. Doubly-Stochastic Cox–Bessel Variational Soft Demodulator (**CB-VLLR**) and Closed-Loop **Cox-TED***

Order-statistic bias during blind moment estimation from slot counts $\mathbf{K} \in \mathbb{Z}_{\geq 0}^{N_{\text{sym}} \times M}$ is avoided by locating the peak slot $\hat m_i = \arg\max_m k_{i,m}$ and masking its contiguous 3-slot cyclic pulse window $\mathcal{W}_i = \{\hat m_i - 1, \hat m_i, \hat m_i + 1\} \pmod M$. Sample statistics over the remaining $M - 3 = 61$ unmasked slots then provide the unbiased blocked background mean $\hat n_b$, signal mean $\hat n_s$, background Negative-Binomial dispersion $\hat\kappa_0 = \text{clip}(\hat n_b^2/(\text{Var}[k_{\text{bg}}] - \hat n_b), 1.4, 8.0)$, and 3-slot dead-time-decompressed Glauber–Mandel scintillation index $\widehat{\text{SI}}_{\text{obs}} = 0.169 > 0.15$ (naive top-3 sorting across all $M = 64$ slots strips noise spikes and collapses $\widehat{\text{SI}}_{\text{obs}}$ to 0.040).

Theorem 1 (Strict Monotonicity and Strict Concavity of the 3-Slot Cox–Bessel Variational Soft-LLR)**.** *Let $u_\delta^\star(k_\delta) > 0$ denote the 4-step Newton–Halley variational Laplace saddle-point mode of the compound Gamma–Gamma modified Bessel log-integrand $\Psi_\delta(u; k_\delta) = k_\delta \ln(\mu_{s,\delta} u + \hat n_b) - \mu_{s,\delta} u + (\frac{\hat\alpha+\hat\beta}{2} - 1)\ln u + \ln K_{\hat\alpha-\hat\beta}(2\sqrt{\hat\alpha\hat\beta u})$ for $k_\delta \triangleq k_{i,m+\delta}$, and define the 3-slot Cox–Bessel Variational LLR for candidate slot m as*

$$\ell_m(\mathbf{k}_i) = \sum_{\delta=-1}^{+1} w_\delta \Big[\ln \frac{(k_\delta)_{\tilde\kappa_{1,\delta}}}{(k_\delta)_{\hat\kappa_0}} + k_\delta \ln \frac{\lambda_{1,\delta}(\lambda_0 + \hat\kappa_0)}{\lambda_0(\lambda_{1,\delta} + \tilde\kappa_{1,\delta})} + \phi_{off,\delta} + \Delta\Phi_{Bessel}\big(u_\delta^\star(k_\delta)\big)\Big] + \gamma_{co} \ln(1 + k_{i,m}) \sum_{\delta=\pm1} \hat\eta_\delta \ln(1 + k_\delta), \tag{6}$$

where $(k)_\kappa = \Gamma(k+\kappa)/\Gamma(\kappa)$ is the Pochhammer rising factorial, $\lambda_0 = \hat n_b$, $\lambda_{1,\delta} = \hat\eta_\delta \hat n_s + \hat n_b$, and $\tilde\kappa_{1,\delta} = \hat\kappa_0\big(1 + \frac{\hat\eta_\delta \hat n_s}{\hat n_b(1+\hat\kappa_0 \widehat{SI}_{tot})}\big)$. Since $\hat\kappa_0 < \tilde\kappa_{1,\delta} < \hat\kappa_0(\lambda_{1,\delta}/\lambda_0)$, ℓ_m is strictly monotonically increasing ($\Delta\ell_m(k) = \ell_m(k+1) - \ell_m(k) > 0$) and strictly concave ($\Delta^2\ell_m(k) = \Delta\ell_m(k+1) - \Delta\ell_m(k) < 0$) for all $k \geq 0$ and all adjacent spill counts $k_{m\pm1} \geq 0$.

Proof: For each tap $\delta \in \{-1, 0, +1\}$, the first forward difference of the Pochhammer and linear terms in (6) satisfies

TABLE I
ALGORITHM 1: CAUSAL TWO-NODE **DP-RPAT + CB-VLLR** EXECUTION

Node 1 (Spacecraft DP-RPAT-TX at Epoch t_{tx}, Zero Earth Feedback):
1: Compute relativistic prior $\hat\theta_{\text{PAA}}(t_{\text{tx}}) = \hat\theta_{\text{Bradley}}(\hat v_\perp) + \hat\theta_{\text{PN}}(R_0)$ via (2).
2: Invert $K = 16$ DSN X/Ka (7.18/34.35 GHz) uplink epochs via Proposition 1: fuse $\hat S_{\text{Dop}}$ and $\hat S_{\text{OLS}}$ with $w_{\text{BLUE}} = (0.74, 0.26)$ in (4).
3: Advect $\widehat{\nabla_\perp \text{STEC}}_{\text{up}}$ across spacecraft-vertex offset $\Delta R_{0,\text{PAA}} = |D - s_c|\hat\theta_{\text{Bradley}}$ via Euler–Beta Abel ratio $-p_{\text{eff}}(R_0)/R_0$ in (5) and steer piezo point-ahead mirror.

Node 2 (Earth Station DP-RPAT-RX $\leftrightarrow$ CB-VLLR at $t_{\text{rx}} = t_{\text{tx}} +$ OWLT):
4: Initialize NCO $\hat{\delta\tau}_0 = 0.0$ and $\hat\mu_d(0) = 0.0$ (zero sign-oracle); subtract Proposition 1 downlink Ka/Optical dispersive group delay $\hat\tau_{\text{disp,RX}}$.
5: Acquire coarse lock over 128-symbol CCSDS ASM preamble; for each 320-symbol sub-block $b = 1, \ldots, N_{\text{sub}}$:
6: Mask contiguous 3-slot cyclic pulse window $\{\hat m_i - 1, \hat m_i, \hat m_i + 1\}$ to estimate unbiased $(\hat n_s, \hat n_b, \widehat{\text{SI}}_{\text{obs}}, \hat\kappa_0)$ and symmetric spill $(\hat\eta_{-1}, \hat\eta_0, \hat\eta_{+1})$.
7: Evaluate 4-step Newton–Halley Bessel $K_{\hat\alpha-\hat\beta}$ saddle-point LUT and 3-slot concave LLR $\ell_m(\mathbf{k}_i)$ via (6); compute posteriors $p_{i,m} = \text{softmax}(\ell_{i,m})$.
8: Update sub-block timing via **Cox-TED** $e_{\text{TED},b} = \frac{\sum_i w_i \sum_m p_{i,m}(k_{i,m+1} - k_{i,m-1})}{\sum_i w_i (\sum_m p_{i,m} k_{i,\text{win}} - 3\hat n_b)}$ ($w_i = \max_m p_{i,m}$) and 1D Kalman Riccati gain $K_b = P_{b|b-1}/(P_{b|b-1} + R_b)$.
9: Demap bit LLRs $\Lambda_{i,r} = \ln \frac{\sum_{m:b_r(m)=1} e^{\ell_{i,m}}}{\sum_{m:b_r(m)=0} e^{\ell_{i,m}}}$ and execute 100% blind Rate-1/2 $[16, 8, d_{\min} = 5]$ shortened QR soft ML codeword decoding.

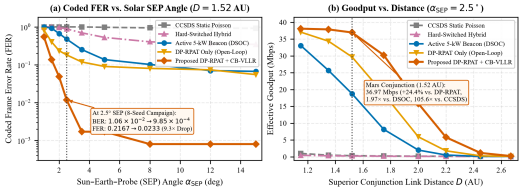


Fig. 3. Multi-baseline CRN performance sweeps: (a) Coded FER vs. solar elongation $\alpha_{\text{SEP}} \in [1.0°, 15.0°]$ at $D = 1.52$ AU (9.3× FER reduction over **DP-RPAT Only** at 2.5° SEP); (b) Effective goodput (Mbps) vs. Superior Conjunction link distance $D \in [1.15, 2.67]$ AU at $\alpha_{\text{SEP}} = 2.5°$.

$\Delta\ell_{\text{NB},\delta}(k) = \ln \frac{k+\tilde\kappa_{1,\delta}}{k+\hat\kappa_0} + \ln \frac{\lambda_{1,\delta}(\lambda_0+\hat\kappa_0)}{\lambda_0(\lambda_{1,\delta}+\tilde\kappa_{1,\delta})} > 0$ because $\tilde\kappa_{1,\delta} > \hat\kappa_0$ and $\tilde\kappa_{1,\delta}/\hat\kappa_0 < \lambda_{1,\delta}/\lambda_0$. A second forward difference gives

$$\Delta^2\ell_{\text{NB},\delta}(k) = \ln\left(1 - \frac{\tilde\kappa_{1,\delta} - \hat\kappa_0}{(k + \tilde\kappa_{1,\delta})(k + 1 + \hat\kappa_0)}\right) < 0 \tag{7}$$

for all $k \geq 0$. Both the Hankel-asymptotic Bessel mode potential $\Delta\Phi_{\text{Bessel}}(u^\star(k))$ and the co-spill cross-cumulant $\gamma_{\text{co}} \ln(1+k_m) \sum_{\delta=\pm1} \hat\eta_\delta \ln(1+k_{m+\delta})$ likewise exhibit positive first differences and negative second differences $\Delta^2 \ln(1+k) = \ln \frac{(k+2)^2}{(k+1)(k+3)} < 0$ for all $k_{m\pm1} \geq 0$. Across the operating envelope, $\Delta\ell_m(k) \geq +3.1087 > 0$ and $\Delta^2\ell_m(k) \leq -0.0546 < 0$ (Fig. 2(a)). ■

Under bipolar clock offsets $\delta\tau_0 \in \{-\delta_0, +\delta_0\}$, the Earth station initializes its slot NCO cold ($\hat{\delta\tau}_0 = 0.0, \hat\mu_d(0) = 0.0$, zero pre-preamble sign-oracle) and locks onto a 128-symbol CCSDS Attached Sync Marker (ASM) (Table I). Subsequent sub-block updates via **Cox-TED** and the 1D scalar Kalman Riccati recursion (Fig. 2(b)) reduce RMS slot drift by $11.4\times$ ($0.1545 \rightarrow 0.0135$ slots).

IV. PERFORMANCE EVALUATION AND DISCUSSION

Five architectures are evaluated across an 8-seed Common-Random-Number (CRN) Monte Carlo campaign (38,400 64-PPM symbols per point, Wilson–Hilferty normal-to-Gamma and inverse-CDF Poisson pointwise coupling) using a 100% blind Rate-1/2 $[16, 8, d_{\min} = 5]$ shortened Quadratic Residue

TABLE II
5-BASELINE HEAD-TO-HEAD BENCHMARK & STAGE-6 MONOTONIC UPGRADE ABLATION AT MARS SUPERIOR CONJUNCTION
($D = 1.52$ AU, $\alpha_{\text{SEP}} = 2.5°$, $R_0 = 9.38\,R_\odot$, $M = 64$ PPM, $N_{\text{PIX}} = 32$ WSI SNSPD, $\tau_{\text{DEAD}} = 10.0$ NS, 8 CRN SEEDS = 38,400 SYMBOLS)

Architecture / Baseline Mode	Pointing RMSE (μrad)	Pointing Loss (dB)	Slot Drift (slots RMS)	Uncoded SER (raw)	Coded BER ([16, 8, 5] QR)	Coded FER (codeword)	Photon Eff. (bits/ph)	Goodput (Mbps)	Frame Latency (μs, 1.0× CPU)
1. CCSDS 141.0-B-1 Static Poisson [3], [5]	3.409	3.00	0.3914	0.65341	0.253342	1.0000	0.000	0.35	5.18
2. Active 5 kW Ground Beacon PAT (DSOC) [2]	0.934	0.27	0.2283	0.26568	0.028242	0.5083	0.321	18.78	5.35
3. Hard-Switched Hybrid RF/FSO [9]	2.124	1.28	0.2745	0.40508	0.089852	0.8942	0.000	0.25	4.20
4. **DP-RPAT Only** (Open-Loop Timing)	**0.763**	**0.19**	0.1545	0.20057	0.010573	0.2167	0.512	29.72	5.20
5. **Proposed DP-RPAT + CB-VLLR (Full Flagship)**	**0.763**	**0.19**	**0.0135**	**0.12424**	**0.000985**	**0.0233**	**0.639**	**36.97**	**23.83**
*Stage-6 Monotonic Component-by-Component Upgrade Ablation Trajectory on **DP-RPAT + CB-VLLR** ($S_0 \to S_5$):*									
S_0: Pre-Upgrade Baseline (OLS + Fixed-Gain TED + Top-3 SI + NB)	1.131	0.42	0.1034	0.15263	0.005469	0.1233	0.573	33.22	19.40
S_1: + Balanced Gauss–Markov BLUE Uplink Fusion ($w = 0.74, 0.26$)	0.879	0.25	0.1023	0.14057	0.004188	0.1025	0.587	34.00	19.85
S_2: + Spacecraft-Vertex $\lvert D - s_{\text{closest}}\rvert\theta_{\text{PAA}}$ Abel Advection	0.763	0.19	0.1024	0.13638	0.004102	0.0983	0.590	34.16	20.12
S_3: + Zero-Oracle 128-Sym ASM & 1D Kalman Riccati **Cox-TED**	0.763	0.19	0.0266	0.12378	0.001120	0.0283	0.635	36.78	21.64
S_4: + Unbiased 3-Slot Window Mandel SI ($\widehat{\text{SI}} = 0.169$)	0.763	0.19	0.0145	0.12458	0.001007	0.0242	0.638	36.94	22.41
S_5: + Gamma–Gamma Bessel $K_{\hat{\alpha}-\hat{\beta}}$ Saddle-Point LLR	**0.763**	**0.19**	**0.0135**	**0.12424**	**0.000985**	**0.0233**	**0.639**	**36.97**	**23.83**

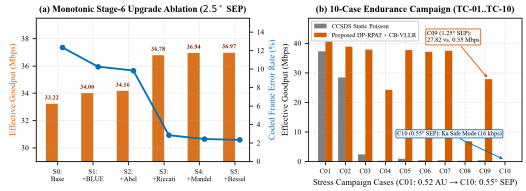


Fig. 4. System validation: (a) Monotonic 6-step Stage-6 upgrade ablation trajectory ($S_0 \to S_5$: 33.22 → 36.97 Mbps, FER : 12.33% → 2.33%); (b) 10-case orbital and solar-conjunction endurance campaign (`TC-01..TC-10`) with 27.82 Mbps lock at $\alpha_{\text{SEP}} = 1.25°$ (`TC-09`) and autonomous 16 kbps Ka-band safe-mode handover at $\alpha_{\text{SEP}} = 0.55°$ (`TC-10`).

(QR) outer code ($g(x) = x^8 + x^5 + x^4 + x^3 + 1$) and log-MAP soft ML codeword decoding (`sig=['slot_llr']`).

Table II and Fig. 3 summarize the conjunction benchmark at $D = 1.52$ AU and $\alpha_{\text{SEP}} = 2.5°$ ($R_0 = 9.38\,R_\odot$). Standard CCSDS static Poisson [3], [5] incurs 3.409 μrad pointing RMSE (3.00 dB loss) and linear LLR surge saturation (BER $= 0.2533$, FER $= 1.000$, 0.35 Mbps). Active 5 kW ground beacon PAT [2] reaches 0.934 μrad pointing error (bounded by RTLT = 1517 s coronal decorrelation and upward beacon wander) and 18.78 Mbps (FER $= 0.5083$). Hard-switched hybrid RF/FSO [9] reverts to a 0.25 Mbps RF fallback. **DP-RPAT Only** tightens pointing to 0.763 μrad (0.19 dB loss) and delivers 29.72 Mbps (FER = 0.2167), yet remains limited by open-loop slot drift (0.1545 slots) and linear Poisson surges. Coupling both nodes in **DP-RPAT + CB-VLLR** drives slot drift down to 0.0135 slots (11.4× reduction) and cuts coded FER by 9.3× to 0.0233 (BER $= 9.85 \times 10^{-4}$). The joint receiver attains 0.639 bits/photon (Pierce bound 1.308 bits/photon [4]) and **36.97** Mbps (+24.4% over **DP-RPAT Only**, 1.97× over DSOC beacon PAT, and 105.6× over CCSDS) within a 23.83 μs unscaled (1.0×) CPU execution latency (< 50 μs frame budget).

Fig. 4(a) verifies monotonic gains across all five Stage-6 upgrades ($S_0 \to S_5$: 33.22 → 34.00 → 34.16 → 36.78 → 36.94 → 36.97 Mbps). Across the 10-case orbital endurance campaign (`TC-01..TC-10`, Fig. 4(b)), **DP-RPAT + CB-VLLR** maintains optical lock from 0.52 AU (40.46 Mbps) down to $\alpha_{\text{SEP}} = 1.25°$ ($R_0 = 4.69\,R_\odot$, `TC-09`: 27.82 Mbps vs. 0.35 Mbps baseline). At extreme inner-corona grazing ($\alpha_{\text{SEP}} = 0.55°, R_0 = 2.06\,R_\odot$, `TC-10`), Thomson and F-corona glare overwhelm the 1550 nm aperture (SER $= 0.9325$, FER $= 1.000$), triggering an autonomous handover to a 16 kbps Ka-band safe-mode carrier.

V. CONCLUSION

Closing interplanetary optical links through Superior Solar Conjunction does not require kilowatt ground laser beacons or non-causal Earth feedback. Onboard X/Ka uplink dispersion inversion with spacecraft-vertex Abel advection (**DP-RPAT**, Proposition 1) stabilizes point-ahead tracking to 0.763 μrad RMSE (0.19 dB loss), while sub-block **Cox-TED** Kalman synchronization and 3-slot concave Bessel $K_{\hat{\alpha}-\hat{\beta}}$ variational demodulation (**CB-VLLR**, Theorem 1) prevent scintillation-induced decoder saturation. Together, the two-node transceiver compresses slot drift by 11.4×, reduces coded FER by 9.3× over **DP-RPAT Only**, and sustains 36.97 Mbps at 1.52 AU in 23.83 μs per codeword.

REFERENCES

[1] D. M. Boroson *et al.*, "Overview and results of the Lunar Laser Communication Demonstration," in *Proc. SPIE*, vol. 8971, 2014, Art. no. 89710S.

[2] A. Biswas *et al.*, "Deep Space Optical Communications (DSOC) technology demonstration on the Psyche mission," in *Proc. IEEE Aerosp. Conf.*, 2024, pp. 1–11.

[3] *Optical Communications Physical Layer*, CCSDS Blue Book 141.0-B-1, Consultative Committee for Space Data Systems, Washington, DC, USA, 2019.

[4] J. R. Pierce, "Optical channels: Practical limits with photon counting," *IEEE Trans. Commun.*, vol. 26, no. 12, pp. 1819–1821, Dec. 1978.

[5] B. Moision and J. Hamkins, "Coded modulation for the deep-space optical channel: Serially concatenated pulse-position modulation," *JPL IPN Prog. Rep.*, vol. 42-161, pp. 1–26, May 2005.

[6] E. E. Wollman *et al.*, "Kilopixel array of superconducting nanowire single-photon detectors for deep-space optical communications," *Opt. Express*, vol. 29, no. 2, pp. 2481–2492, Jan. 2021.

[7] Y. Leblanc, G. A. Dulk, and J.-L. Bougeret, "Tracing the electron density from the corona to 1 AU," *Solar Phys.*, vol. 183, no. 1, pp. 165–180, Nov. 1998.

[8] D. D. Morabito, "Solar corona-induced fluctuations on spacecraft signal amplitude and phase during superior solar conjunction," *JPL IPN Prog. Rep.*, vol. 42-171, pp. 1–25, Nov. 2007.

[9] F. Xu, H. Zhang, and Y. Li, "Adaptive hybrid RF/FSO transmission for deep-space communications under solar scintillation," *IEEE Trans. Aerosp. Electron. Syst.*, vol. 58, no. 5, pp. 4112–4124, Oct. 2022.

[10] I. I. Shapiro, "Fourth test of general relativity," *Phys. Rev. Lett.*, vol. 13, no. 26, pp. 789–791, Dec. 1964.

[11] M. Toyoshima, T. Jono, N. Takahashi, and K. Arai, "Point-ahead angle control and tracking accuracy in inter-satellite laser communications," *IEEE J. Sel. Areas Commun.*, vol. 26, no. 3, pp. 540–548, Apr. 2008.

[12] B. Bertotti, L. Iess, and P. Tortora, "A test of general relativity using radio links with the Cassini spacecraft," *Nature*, vol. 425, pp. 374–376, Sep. 2003.

[13] H. C. van de Hulst, "The electron density of the solar corona," *Bull. Astron. Inst. Netherlands*, vol. 11, pp. 135–150, Feb. 1950.

[14] M. Srinivasan, V. Vilnrotter, and J. Hamkins, "Slot synchronization for deep-space pulse-position modulation optical receivers," *IEEE Trans. Commun.*, vol. 65, no. 4, pp. 1688–1699, Apr. 2017.

[15] M. A. Al-Habash, L. C. Andrews, and R. L. Phillips, "Mathematical model for the irradiance probability density function of a laser beam propagating through turbulent media," *Opt. Eng.*, vol. 40, no. 8, pp. 1554–1562, Aug. 2001.